Lattice parameter and orientation of xenon on graphite at low pressures

M. Hamichi, A. Q. D. Faisal, J. A. Venables,* and R. Kariotis†
School of Mathematical and Physical Sciences, University of Sussex, Brighton BN1 9QH, England
(Received 11 March 1988)

A study of xenon adsorbed on (0001) graphite has been performed using transmission high-energy electron diffraction (THEED). The single crystal diffraction patterns have been obtained at a range of pressures $1.8\times10^{-8}<p<1.8\times10^{-5}$ Torr and temperatures $50<T<80$ K, which covers the incommensurate monolayer, commensurate monolayer, and bilayer phases. The lattice-parameter misfit, m, has been measured to $\pm0.1\%$, and the misorientation θ to $\pm0.1°$ accuracy. The misfit in the incommensurate phase is parametrized as $m=B(T-T_0)^{\beta}$, with $\beta=0.80\pm0.03$ and B and T_0 as functions of $\log_{10}(p)$. A tricritical point (I-C monolayer, bilayer) is observed at $p=2.0\pm0.5\times10^{-6}$ Torr, $T=62.5\pm1$ K. The small misorientation ($0\le\theta<0.4°$) is a well-defined function of m in the monolayer phase, with an aligned-rotated transition at $m=1.5\pm0.5\%$. These features are compared with other experiments and with theoretical predictions.

I. INTRODUCTION

Structures and phase transitions of rare gases physisorbed on the basal plane of graphite have been an area of extensive research during the last two decades. Various techniques have been used to study the heavier rare gases including, for the case of Xe, thermodynamic measurements,[1–4] electron diffraction in the form of low-energy electron diffraction (LEED),[5–7] reflection high-energy electron diffraction (RHEED),[8] and transmission high-energy electron diffraction (THEED),[9–12] x-ray,[13–23] and light atom[24–32] diffraction. Several authors have reviewed much of this work in the context of surveys of adsorption of the heavier rare gases and simple molecules on graphite.[33–38]

Since the original explorative work of Thomy and Duval,[1] a number of different phases and phase transitions have been discovered. As a result, a large amount of data are now available, and the phase diagrams of these gases have become well known. In particular, the gases show a wide region of the $(\log_{10}p, T^{-1})$ plane where an adsorbed solid monolayer is stable. This monolayer can be either commensurate (C) or incommensurate (I) with the underlying basal plane of graphite. The incommensurate phase can either be aligned with the graphite lattice (IA phase) or rotated (IR phase). The IR phase was first observed for Ar on graphite,[39] and has since been observed for Kr (Refs. 11 and 40) and Ne.[41]

For xenon on graphite at low pressures, previous transmission high-energy electron diffraction (THEED) investigations[9–11] showed that the xenon first condensed into an I phase with a positive misfit with respect to the graphite. As the temperature was reduced at constant pressure, the misfit decreased towards zero indicating an I-C transition. It has subsequently been claimed, on the basis of oriented-powder x-ray diffraction work,[22] that the C phase did not exist, but rather a striped phase (one-dimensional misfit) existed at low pressures near monolayer coverage; various other aspects of the I-C and monolayer-bilayer transitions were also queried.

We have now performed new experiments on this Xe-graphite system using a THEED camera, modified to contain a uhv environmental chamber. We have confirmed the existence of the I-C transition, and obtained better accuracy than the previous misfit measurements.[11] As reported here, we have extended these measurements to a wider range of pressure and temperature, spanning the I-C and monolayer-bilayer transitions. The relevant section of the $(\log_{10}p, T^{-1})$ phase diagram is shown in Fig. 1.

The main results of this work are that we have not seen any evidence of a striped phase in the whole range of the phase diagram studied. The data indicate a tricritical point at the coexistence of the I, C, and bilayer phases. New bilayer data confirm the previous LEED data.[7] The onset of small amounts of rotation was also seen at small positive misfit, indicating the existence of an IA-IR transition. This is compared with the most recent single crystal x-ray data.[22,23]

The structure of the paper is as follows. In Sec. II, we briefly describe the main experimental modifications including the new environmental chamber, the sample holder, and the gas handling system. A description of the sample preparation, misfit, and rotation measurement procedures is also given. Section III describes the lattice parameter and rotation results, and power-law fits are obtained from these data and discussed. In Sec. IV the results are compared to previous THEED and x-ray results and a phase diagram is constructed.

II. EXPERIMENTAL TECHNIQUES

A. Apparatus

The previous THEED experiments of Xe on graphite[11] were carried out in the pressure range $5.0\times10^{-8}<p<1.5\times10^{-6}$ Torr; the system relied on local cryogenic pumping to achieve a good base pressure. In order to extend this work to a much wider pressure range, several modifications have been made, including a

 ©1989 The American Physical Society

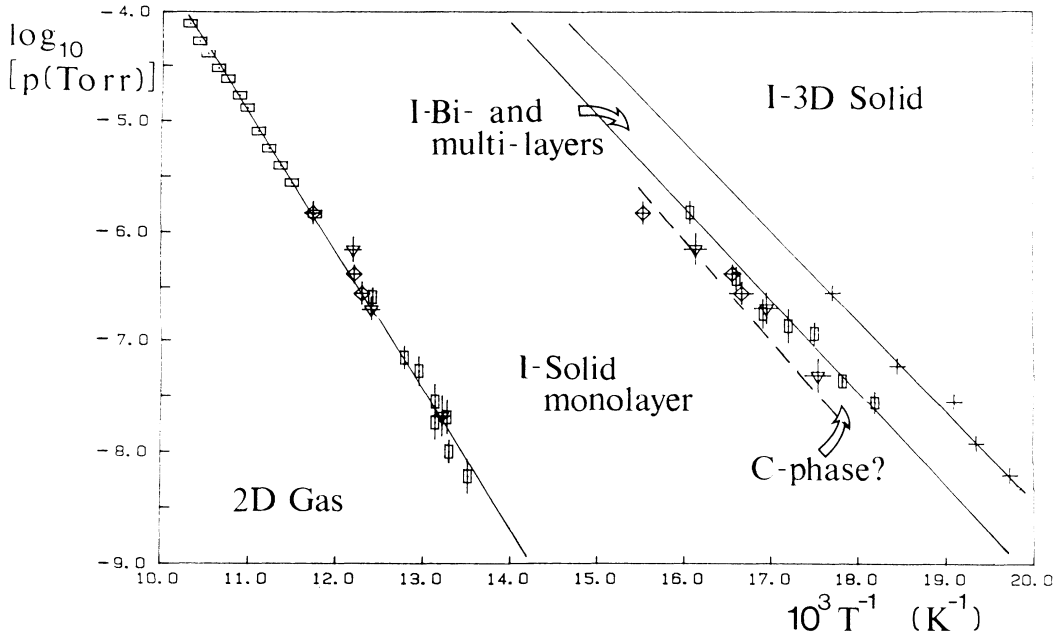

FIG. 1. Phase diagram of xenon on graphite in the temperature and pressure region studied, prior to this work. The following phase transition data are shown: Monolayer and bilayer LEED data from Suzanne *et al.* (Ref. 6, horizontal rectangle) and (Ref. 7, vertical rectangle); THEED data from Venables *et al.* (Ref. 10, inverted triangle), Schabes-Retchkiman and Venables (Ref. 11, diamond). The crosses are the lowest pressure quartz crystal bulk condensation measurements of Levenson (Ref. 42).

new uhv environmental chamber, sample holder, and gas handling system. A more detailed account is published elsewhere,[43] but the following description is sufficient to understand the capabilities of the apparatus. We are using a heavily modified Hitachi HU.11B transmission electron microscope (TEM), dating from 1964, to obtain the electron beam and to record the diffraction patterns, but any (nonautomatic, 100 kV) TEM would do in its place.

1. Environmental chamber design

The basic requirement of the design was to have a chamber which could be operated at uhv, in order to clean the sample, and at a controllable (high) pressure to do the experiments. A schematic cross section of the chamber is shown in Fig. 2. The incident beam (E) passes through the top aperture (A) through the sample (S) and then leaves the uhv chamber through the bottom aperture (B) located just above a new objective lens (O). The apertures are mounted on a ring of four miniflanges. One of these is occupied by a small window so that the sample can be seen. The chamber is made from a 63-mm diameter tube which can be removed from the right-hand side of the microscope if necessary. An extension block (C) between the tube and the original microscope chamber was provided for aperture adjustments during the alignment procedures. The left-hand side of the chamber (P) is connected to the uhv pumping system, which consists of 50 $1s^{-1}$ turbomolecular pump (backed by the microscope vacuum), and titanium sublimation pump. A gate valve isolates the turbopump from the uhv cell during the experiment.

The critical choices involve the sizes of the apertures A and B and the distances $SA=10$ mm and $SB=7$ mm. The size of the bottom aperture B was chosen to be large enough to allow the second-order (20) Xe reflections through the aperture at 100 kV: this resulted in a 400-μm diameter aperture being chosen. In principle, the top aperture A could be smaller, but experiments with a 250-μm aperture gave difficulties with alignment; the experiments were done with another 400-μm aperture. The distance AB limits, due to gas scattering of the electron beam, the upper pressure available to around 1 Torr. The area of the apertures clearly determines the leak rate and the effective (impurity) background pressure at the sample.[43]

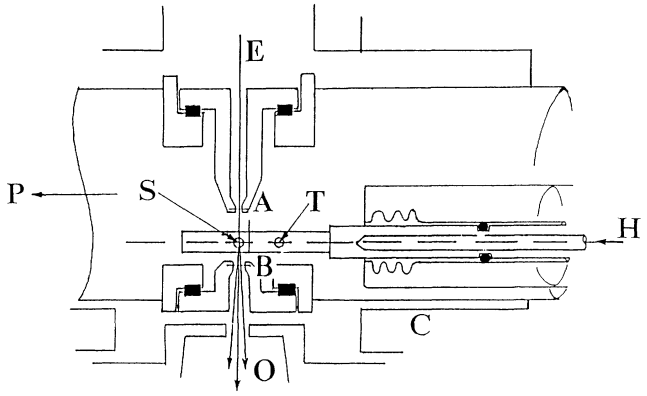

FIG. 2. Schematic diagram of the new environmental chamber and sample holder: A and B, apertures; C, extension block; E, electron beam; H, helium flow cryostat; O, objective lens; P, pumps; S, sample. See text for discussion.

With the apertures chosen, a pressure ratio of about 3000 can be maintained across them. This means that we can run the apparatus in one of two modes. To clean the sample we run the chamber under uhv conditions at $<10^{-9}$ Torr, with the pressure in the main external chamber below 10^{-6} Torr. Alternatively, we can flood the environmental chamber with the gas concerned and allow the external chamber pressure to rise to $\sim 10^{-3}$ Torr. Thus the highest pressure achievable is a few Torr; the pressure limits caused by gas scattering and pumping speeds are of the same order. The important point is that a pressure range of $10^{-9} \lesssim p \lesssim 1$ Torr is achievable, which is wider than for any other electron diffraction apparatus currently used for adsorption studies.

2. Sample holder design and temperature measurements

An uhv-compatible side-entry low-temperature holder was designed, as shown schematically in Fig. 2. The main requirements were to achieve a lower temperature of 30 K, with a sample heating temperature for cleaning of up to 1500 °C. It consists of two parts. The first part is made of a stainless steel double "O"-ring rod fitted with a vacuum jacket, which acted as a continuous flow helium cryostat (H); this terminates in a Cu-Te cold finger. The second part of the holder consists of a cooling block and sample support, both made of Cu-Te. The cooling block is clamped to the cold finger ensuring a good thermal contact. A silicon diode sensor was attached on the cooling block for temperature measurements (T). Good thermal contact between the diode and the cooling block was ensured by using silver dag. A small heater was also wound on the cooling block to regulate the temperature.

The sample, S in Fig. 2, was mounted on a separate support piece. First a tungsten microscope grid (approx. 3×1.5 mm^2), which had been cut down to maximize its resistance, was spot welded to a tantalum tag. The tag is then screwed onto the support piece. One end of the sample was insulated from the rest of the holder by machinable glass ceramic insulators. This was provided for sample cleaning. A current could be passed through the tag, then through the specimen to earth. After picking up the sample on the support piece, the whole assembly was fixed with two screws onto the cooling block. To ensure good thermal contact, a thin sheet of gold leaf was placed between the support piece and the cooling block. All the wires were fed into the sample chamber via an electrical feedthrough and were heat sinked to the cooling block, in order to minimize the heat input to the sample.

The temperature was measured by a silicon diode (Lake Shore Cryogenics Inc., Model DT500K), calibrated at Sussex against a calibrated gold-iron versus chromel thermocouple to better than 0.1 K. The voltage and the temperature of the sample were displayed on a DRC-82C temperature controller. Temperature control was effected by changing the rate of the helium flow using a needle valve in the helium pumping line. Temperature stability of ±0.1 K was achieved routinely.

3. Gas handling system and pressure measurements

A simple gas handling system was manufactured by Cryogenic and Vacuum Technology (CVT) Ltd. The gas line was isolated from the environmental chamber by a metal valve and a needle valve. A Baratron gauge (MKS Instruments, Inc.) was used to measure pressures up to 1000 Torr. The Xe gas used was of nominal purity 99.997% (British Oxygen Corporation grade X), the main impurity being krypton. To preserve the purity of the gas we cleaned the gas line as follows. After isolating the gas line from the environmental chamber is was roughed by a liquid-N_2–cooled sorption pump. The gas line was then connected to the uhv chamber through the metal valves and baked. After reaching a good vacuum ($\sim 10^{-8}$ Torr) the gas line was isolated and filled with gas to ~ 500 Torr.

During the experiments the pressure was measured by a second Baratron head (10^{-3}–1 Torr) and an ionization gauge, with calibration of the ionization head against the Baratron, taking account of the xenon sensitivity factor of 2.78 with respect to N_2.[44] The titanium sublimation pump was used to keep the rare gases clean, and a residual gas analyzer was available to monitor gas purity.

The pressure was typically kept constant in an experimental run as the temperature was varied. For comparison with true equilibrium adsorption, a thermomolecular correction factor $\sim T^{1/2}$ should in principle be made. However, as in previous experiments,[11] this has not been done, since it has an unknown magnitude which depends on the vapor temperature near the sample. Since the sample holder is much smaller than the enclosure, the variation in effective pressure at the sample will be small over the range of T explored. During a particular run the pressure was kept constant within $\pm15\%$. Our best estimate is that the absolute pressure is known to better than $\pm30\%$ with relative errors of order $\pm15\%$. For example, we obtained agreement at this level with previous measurements of the bilayer condensation pressure, as shown later in Fig. 8.

B. Sample preparation

The method followed to prepare the graphite specimen is the same as the one used in previous THEED experiments.[11] Two cleaned microscope slides were coated with 5% weight-to-volume solution of polyvinyl pyrrolidone (PVP) in distilled water. Just before the PVP cement dried, a fairly thick piece of graphite (~0.1 mm) held by a double-sided adhesive (sellotape) was glided onto the slides causing cleavage to occur. This was further cleaved until the remaining piece as seen under a light microscope showed large homogeneous areas transparent to light. The thinnest films (a few tens of nanometers) were transparent and were light grey in color in transmitted light. The large thin areas were then floated on a warm distilled water bath and picked up onto a prepared tungsten grid using the support piece. The graphite sticks firmly to the grid with good thermal contact.

C. Run procedures

After reaching a vacuum of $\sim1\times10^{-9}$ Torr, the sample was cooled to a temperature of ~40 K. The liquid helium was transferred from a 100 L Dewar via a transfer tube down the axis of the side entry rod. A current of ~4.5 A was then passed through the tungsten grid to

clean the graphite sample for 5–10 min. A yellow glow was observed through the small window at the front of the chamber. The heating caused the pressure to rise momentarily up to 1.10^{-7} Torr. The sample was then flashed for 10 s at ~ 5 Å. After cooling down the background pressure was 1×10^{-9} Torr. A pressure of gas was then introduced into the chamber through the needle valve. After fixing the pressure, the temperature was lowered very slowly and diffraction patterns were recorded on SP352 (Ilford) films at different sample temperatures. The exposure time was 10 s, and the cooling rate typically $\lesssim 0.5$ K/min.

D. Lattice-parameter (misfit) measurements

The misfit, defined as the relative difference between the lattice parameter of Xe, a_x, and the graphite substrate, a_c, is given by[11]

$$m=\frac{a_x-a_c}{a_c}=\frac{g_c\{10\bar{1}0\}-g_x\{11\}}{g_x\{11\}}=\frac{\Delta_g}{g_x}\ , \qquad (1)$$

where g_x and g_c are, respectively, the reciprocal-lattice vectors of the Xe and graphite. The misfit was measured by projecting the diffraction pattern onto a screen at about 15 times magnification. Three methods, differing only in detail, were used, as shown in Fig. 3.

The first method was used by Schabes-Retchkiman.[11] A triangular lattice was drawn between the {10} Xe spots and then a straight line was drawn through the {20} Xe spots. In this case, $g_x=g_1$ corresponds to half the distance between two opposite lines drawn through the {20} spots; Δg is Δg_1 as shown in Fig. 3. A second method was used in the absence of the second-order Xe spots. The center of the pattern is first determined by drawing a triangular lattice between the {10} spots. The three g_x values and the corresponding Δg's (only Δg_2 is shown in Fig. 3) were measured, and the misfit was found by taking the average of the misfits in the three directions. The average accuracy to using these two methods was $\Delta m=\pm0.2\%$. The misfit for the above methods was corrected at small values for systematic errors caused by radial distortion in the projector lens.[43]

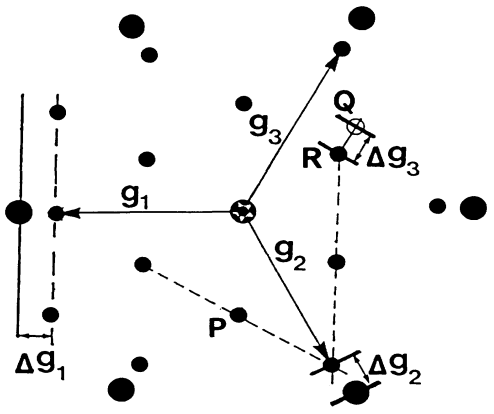

FIG. 3. Methods of misfit measurement: 1, 2, and 3, as discussed in the text. Large solid circle, graphite {10$\bar{1}$0} spots; small solid circle, Xe {10}, {11}, and {20} spots; open circle, double diffraction spots. The Xe diffraction spot P is diffracted by graphite to the doubly diffracted spot Q.

The third method used double diffraction between xenon and graphite when it was present, as discussed by Faisal *et al.*[12] previously. Two parallel straight lines were drawn, one through the center of the double diffraction spot Q and the other through the neighboring {10} Xe spot R. The lines were perpendicular to PR where P is the {10} Xe spot doubly diffracted by graphite to Q. The distances PQ and PR give $g_c\{10\bar{1}0\}$ and $g_x\{11\}=g_3$, respectively, and hence the misfit from Eq. (1). An accuracy of $\pm0.1\%$ was achieved using this method.

E. Densitometry procedures

The small angle of misorientation between xenon and graphite was measured using a computer-controlled densitometer at the Royal Greenwich Observatory at Herstmonceux, Sussex. The procedure is, in principle, the same as the one used by Schabes-Retchkiman[11] to measure diffracted intensities. In our case, a raster of (128×128) pixels was scanned across a {10} Xe spot in 20-μm steps. Care was taken to make sure that the raster was centered on the spot, and the x and y axes were parallel and tangential to the graphite lattice. The (128×128) measurements of photographic densities were stored on a magnetic tape as integers and then transferred onto disk at Sussex University where data analysis was performed. This is described in detail in Sec. III D.

III. RESULTS AND DISCUSSION

A. Lattice-parameter measurements

In order to clarify some aspects of the *I-C* transition of xenon on graphite, we performed new experiments using the THEED camera described in Sec. II. The experiments were carried out in the pressure range of $1.8\pm0.5\times10^{-8}\le p\le1.8\pm0.5\times10^{-5}$ Torr and temperature range of $50\le T\le80$ K. All the experiments were done at constant pressure by lowering the temperature. After recording the diffraction patterns, the misfit was measured as described earlier. The measurements are shown in Fig. 4 where the misfit is plotted versus the temperature for nine different pressures. The lines are power-law fits which are discussed below.

As one can see from Fig. 4, the misfit decrease monotonically as the temperature is lowered at constant pressure. The data can be divided into two groups. In the pressure range $1.8\pm0.5\times10^{-8}\le p<1.8\times10^{-6}$ Torr, the misfit decreases continuously from a value of around 6% near the gas-solid transition, to a value of 0.0 ± 0.2 %, in a continuous manner. This is characteristic of a second-order *I-C* transition. Then the misfit increases abruptly to a value of 2.2 ± 0.1 % characteristic of a first-order transition from the commensurate monolayer phase to the bilayer phase. Multilayers have essentially the same

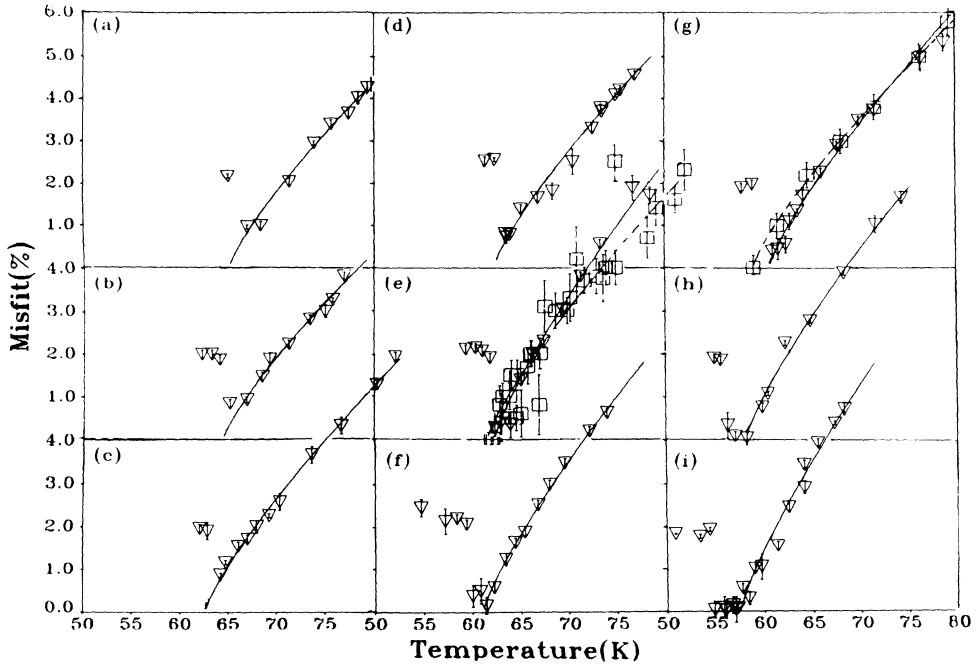

FIG. 4. Misfit vs temperature measured for nine fixed pressures, indicated in panels (a)–(i). The lines are power law fits discussed in the text. For panels (e) and (g) previous data from Ref. 11 are also shown (squares) with similar power-law fits (dashed lines). The pressures are in descending order, in Torr, as follows: (a) 1.8×10^{-5}, (b) 3.6×10^{-6}, (c) 2.9×10^{-6}, (d) 1.8×10^{-6}, (e) 7.2×10^{-7}, (f) 3.6×10^{-7}, (g) 1.8×10^{-7}, (h) 7.2×10^{-8}, (i) 1.8×10^{-8}. See text for discussion.

lattice parameter. One can notice that as the pressure is decreased the *I-C* transition temperature decreases, whereas the width of the commensurate region increases. For the lowest pressure studied, $p=1.8\times10^{-8}$ Torr, this width is equal to 2.5±0.5 K.

For the second group of data, at pressures $p\geq1.8\pm0.5\times10^{-6}$ Torr, we do not see the zero misfit condition. The misfit decreases monotonically to the lowest measured value of 0.5–0.9 % without reaching the zero state. Then it rises discontinuously to the bilayer value of 2.2%. This confirms previous work[13] which revealed that at high pressures the Xe monolayer is incommensurate at the monolayer-bilayer transition. Consequently, a tricritical point[45] exists at the coexistence of the incommensurate, commensurate monolayer, and bilayer phases. We determined the position of this tricritical point to be at 62.5±1 K at a pressure of $2.0\pm0.5\times10^{-6}$ Torr in the T^{-1}, $\log_{10}p$ plane.

B. Misfit data analysis and discussion

The misfit data were fitted to a power-law formula of the form

$$m=B(T-T_0)^{\beta}\ . \tag{2}$$

The fitted curves are represented by the solid lines in Fig. 4. This was done by fixing $\beta=0.8$ and choosing the values of B and T_0 by the least-squares method. By varying β, but keeping it constant for all the data, we could see that $\beta=0.80\pm0.03$ was the most sensible choice. The curves fit the data points with an rms error of 0.05%, which is better than the typical measurement error.

The values of B and T_0^{-1} so determined are plotted in Fig. 5. Both B and T_0^{-1} increase as the pressure is decreased. Although there is some scatter, particularly for B, we have chosen to fit these dependencies in the same two groups, at pressures above and below the tricritical point. The least-squares fits

$$B=B_0+B_1x,\quad T_0^{-1}=C_0+C_1x\ , \tag{3}$$

where $x=-\log_{10}p$, are shown in Fig. 5.

A comparison with previous THEED data can be made by referring to Fig. 4. The misfit data for two pressures ($p=1.8\times10^{-7}$ Torr and $p=7.2\times10^{-7}$ Torr) from Ref. 11 are plotted together with this work. In both cases, the zero misfit state is attained before the bilayer forms, characteristic of a second-order *I-C* transition. Previous THEED data at $p=1.5\times10^{-6}$ Torr (not shown) showed that the misfit goes to zero as the temperature was lowered. Our data at $p=2.9\times10^{-6}$ Torr and above shows that the misfit does not go continuously to zero, since the extrapolated line intersects the temperature axis at a temperature where the bilayer is observed. The two sets of data were fitted with the same power law, shown as dashed and solid lines in Fig. 4. From the power-law fit, we obtained $B=0.65$ for our data at $p=7.2\times10^{-7}$ Torr corresponding to point *F* in Fig. 5. The data from Ref. 11 at $p=7.0\times10^{-7}$ Torr gave a value of $B=0.53$ corresponding to point *S* in Fig. 5; these data are consistent with ours if point *F* is ignored. The data at $p=1.8\times10^{-7}$ Torr show a small shift near the *I-C* transition. In this case our accuracy appears to be su-

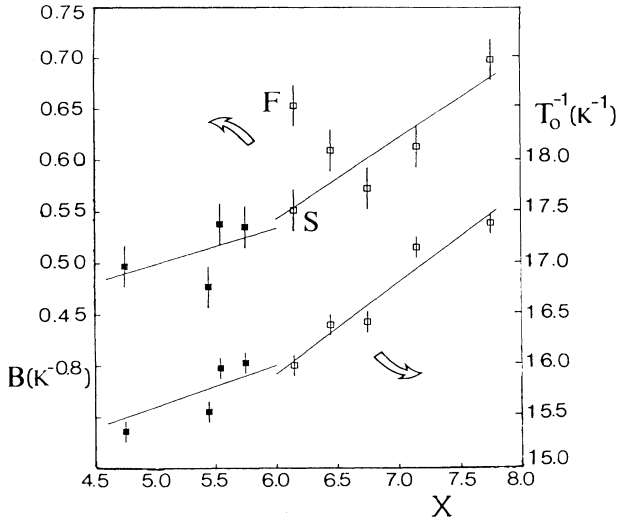

FIG. 5. Values of B and T_0^{-1} from the power-law fit of Eq. (2), as functions of $x=-\log_{10}p$. See text for discussion.

perior. The data set of Fig. 4 shows that there is a tricritical point (I, C, monolayer, and bilayer) at $p=2.0\pm0.5\times10^{-6}$ Torr and $T=62.5\pm1$ K. It is not possible from these data to say unequivocally that there is no commensurate phase above this temperature and pressure. However, if there is, it must exist over a very narrow range of temperature (<0.5 K) at fixed pressure, and be formed in a first-order transition. This is discussed further in Sec. IV.

C. Rotation results

Novaco and McTague[46] first predicted that an incommensurate overlayer could reduce the strain energy caused by the substrate by rotating out of parallel alignment. Shiba[47] included the effect of domain wall formation and predicted the existence of a finite critical misfit for the onset of rotation. Experimentally, the first IR-IA transition was observed in Ar on graphite.[39] Using LEED, Fain, Chinn, and Diehl[40] observed that Kr adsorbed on graphite also undergoes an IR-IA transition suggesting the existence of a finite misfit for the onset of rotation. Schabes-Retchkiman[11] also revealed the existence of the IR-IA transition for Kr but found no rotation in the case of Xe. Recent single-crystal x-ray-diffraction work[20,21,23] has seen evidence for the rotated phase. In particular Hong *et al.*[23] reported that a Xe monolayer undergoes an IR-IA transition with decreasing temperature, in the temperature range of interest.

In the present work, we also observed a small misorientation of the Xe monolayer with respect to the graphite substrate, using densitometry of the Xe {10} spot shapes. The relevant data are shown in Figs. 6 and 7. Figures 6(a) and 6(b) show plots of the misorientation θ as a function of misfit; the lines are least-squares square-root fits. In Fig. 6(a) two pressures above the tricritical point are shown. The angle of rotation θ decreases continuously as the misfit decreases reaching a zero state at a critical misfit of 1.5 ± 0.5 %. Similar behavior is seen in Fig. 6(b) where two pressures below the tricritical point are shown. The fits, discussed below, show strong evidence for the onset of the rotated phase at finite misfit as envisaged by Shiba.[47] However, note how small the misorientation is ($0<\theta<0.4°$), which we have determined to an accuracy of around 0.1°. There is also evidence, from the radial width of the spots shown in Figs. 6(c) and 6(d), that the films become somewhat more disordered as the misfit is reduced. These features are discussed below.

D. Rotation data analysis and discussion

The photographic densities of the Xe {10} spots were measured using a computer controlled densitometer as discussed in Sec. II E. The data were then transferred to Sussex University where a detailed analysis was performed using Fortran routines written for this purpose. First the data were smoothed using a (5×5) convolution program. The densities were then converted to intensities using the photographic calibration previously developed.[11] The background was then subtracted by taking the average of 16 points at the four corners of the raster by linear interpolation, and a contour plot produced. An example is shown in Fig. 7(a) which corresponds to point A in Fig. 6(a). Sections along the radial (x) and tangential (y) directions were then drawn [Figs. 7(b) and 7(c)] and fitted to various functions.

The spot intensities are a relatively good fit to a two-dimensional Gaussian

$$I(x,y)=A\exp[-(x-x_0)^2/2\sigma_x^2-(y-y_0)^2/2\sigma_y^2]\ . \quad (4)$$

Figures 7(b) and 7(c) show the x and y cuts of this function, where σ_x and σ_y were determined from central sections of the data by a least-squares fit to the peak. The misorientation data of Fig. 6 were obtained by taking

$$\theta=(\sigma_y-\sigma_x)/g_x\{10\}\ , \quad (5)$$

which is the simplest measure of misorientation based on Eq. (4), and is the same as used previously.[11] The spot shapes clearly indicate a distribution of misorientation, and other fits such as Lorentzians[16,17,19] or split (e.g., two-center Gaussians) are being investigated.

The data of Figs. 6(a) and 6(b) show considerable scatter but they also show convincing evidence for an IA-IR transition at $m_0=1.5\pm0.5\%$ in agreement with the most recent x-ray work.[23] The least-squares fit to a square-root law shown in Figs. 6(a) and 6(b) has a low variance by comparison with other power laws. For comparison the x-ray data show similar curves, with slightly larger θ values and $m_0=0.033/1.70\equiv1.9\%$ with error $\pm0.3\%$. So we are undoubtedly seeing the same phenomenon, differences in θ probably being due to different measures of the rotation angle. As noted by these workers[23] the absolute value of the rotation is smaller than that envisaged by Shiba,[47] although the form of the curve is similar. We are exploring the possibility that this is another consequence of strong anharmonicity in the Xe layer.[11,48]

The radial spot widths σ_x shown in Figs. 6(c) and 6(d) show an increase as the misfit decreases, from around 75

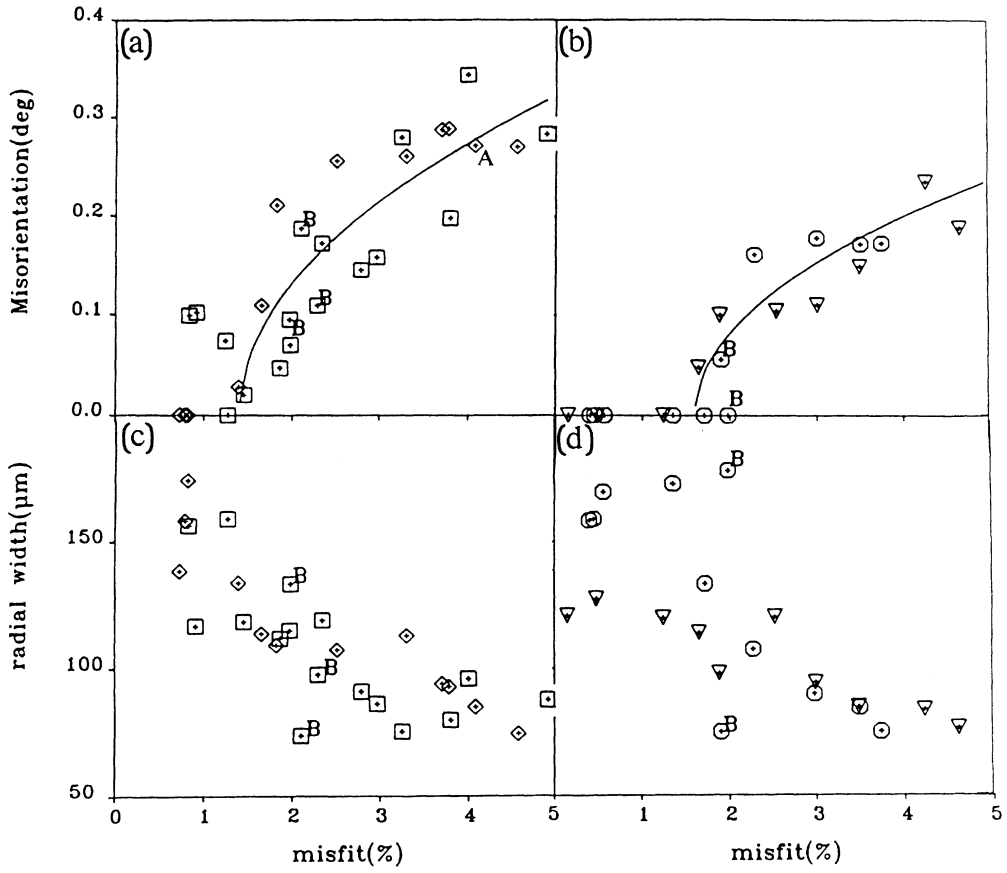

FIG. 6. (a) and (b) misorientation θ vs misfit m; (c) and (d) radial width σ_x vs m. Panels (a) and (c) are at pressures above the tricritical point: $p = 3.6\times10^{-6}$, 1.8×10^{-6} Torr; panels (b) and (d) below tricritical point, $p = 3.6\times10^{-7}$, 1.8×10^{-7} Torr. The point shown as A corresponds to the data of Fig. 7; points B are in the bilayer regime. The lines in panels (a) and (b) are the best square-root functions to fit the data. The points shown as zero rotation are not included in the fit; these eleven points are zero within experimental error, having a mean rotation of $-0.035°$ and standard deviation 0.025°. See text for discussion.

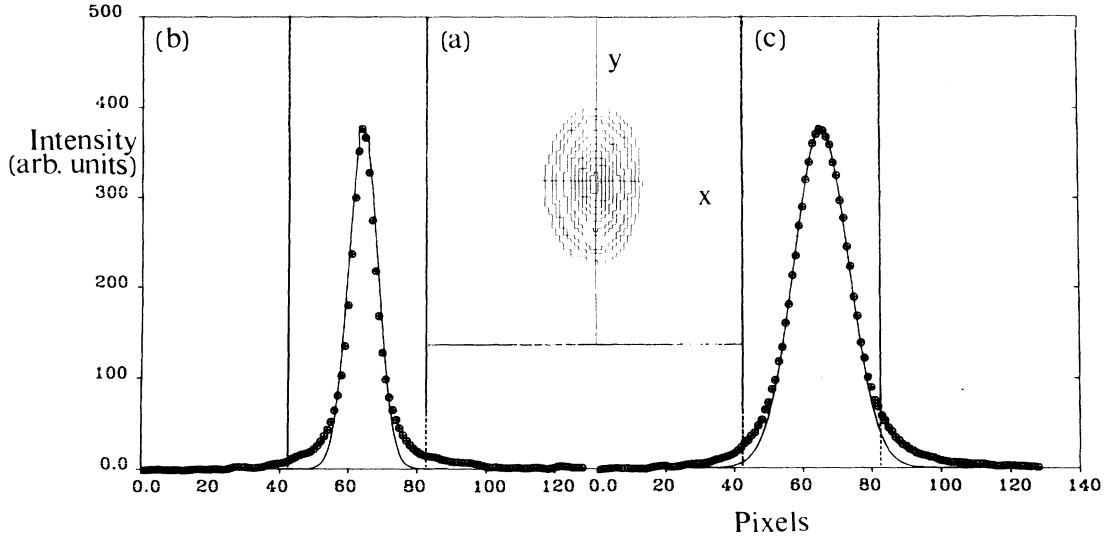

FIG. 7. (a) Shape of spot corresponding to point A on Fig. 6; (b) and (c) tangential and radial scans through this spot with best Gaussian fit within the central channels (vertical lines). See text for discussion.

to 150 μm. This width results both from the positional order in the film, and, as discussed previously,[11] from the coherence of the incident beam; assuming perfect coherence will underestimate the extent of order, perhaps severely. However, these measurements of σ_x can be translated directly into a half width at half maximum (HWHM), as expressed for example in Ref. 38, σ_h, as

$$\sigma_h = (2\log_{10}2)^{1/2}(\sigma_x/g_x)1.701\ (\text{Å}^{-1})\ . \quad (6)$$

With $g_x = 12.5$ mm on the diffraction pattern as recorded, σ_h is in the range $1.2\text{–}2.4\times10^{-2}$ (Å^{-1}). The coherently diffracting domains are thus greater than $2\pi/\sigma_h \sim 600\text{–}300$ Å, possibly much greater. However, the increase in width is almost certainly due to a decrease in order, as the temperature is lowered towards the *I-C* transition. Whether this is a thermodynamic effect, associated with the entropy of domain wall configuration or motion, or an effect due to increasingly sluggish kinetics is not entirely clear. There is considerable theoretical interest in equilibrium disorder near *I-C* transitions, which we discuss in Sec. IV. However, all the present data have been taken by decreasing the temperature at constant pressure, so the disorder could in principle be either thermodynamic or kinetic in origin. Sluggish kinetics and irreversibility in the IA-IR transition have been reported by the x-ray workers.[20,23] Further experimental work is in progress on these points.

E. Monolayer-bilayer transition

The monolayer-bilayer transition was investigated in the same region of the phase diagram. Schabes-Retchkiman and Venables[11] measured a misfit of 2.5±0.3 % for both the bilayer and bulk regimes. Our revised value is 2.2±0.1 %, similar to theirs within experimental error. As previously noticed, two different transitions were observed. Above the tricritical point, the transition occurs from an incommensurate monolayer to the bilayer. Below the tricritical point, the monolayer undergoes first an *I-C* transition, and then an incommensurate bilayer forms with an abrupt rise of the misfit. The measured misfit was found to be temperature independent within our error in both multilayer and bulk crystal regimes. As seen in Figs. 6(c) and 6(d) a rather wide range of radial spot widths was observed. This might be due to instrumental adjustment, but it seems more likely that it is due to different amounts of disorder.

IV. THE PHASE DIAGRAM AT LOW PRESSURES

In this section we compare our results briefly with other experimental studies and with theory. Of the experimental work only the x-ray and THEED results have sufficient resolution, in misfit and misorientation, to warrant a detailed comparison. The phase diagram in the pressure and temperature region of interest is shown in Fig. 8. Here we use our data shown in Figs. 4–6 to indicate some details of this diagram.

We can construct isosteres in the monolayer regime from the data of Fig. 4 using Eqs. (2) and (3), on the assumption that vacancies and second layer atoms are unimportant in this temperature range, which is thought to be the case.[49,50] In that case, the coverage (or areal density) n is given by

$$n = (1+m)^{-2}\ , \quad (7)$$

where $n=1$ corresponds to the C phase. The lines for

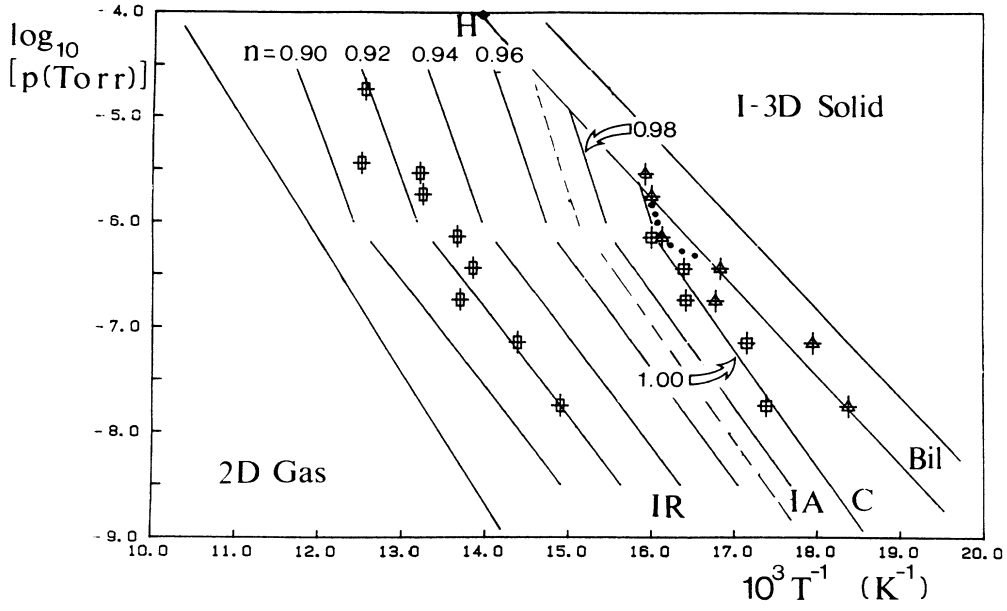

FIG. 8. Phase diagram incorporating the results of the present work. Data points from experimental fits to coverage $n=0.92$ (vertical rectangle), $n=1$ (□) and first appearance of the bilayer (△). See text for discussion.

$n=0.92$–1.00 in steps $\Delta n=0.02$ are shown in Fig. 8. The points corresponding to the fitted lines of Fig. 4 (individual B and T_0 values for each pressure from Fig. 5) are shown in Fig. 8 also for $n=0.92$ and $n=1.00$ (i.e., the I-C transition). Although we have fitted the data in the two groups above and below $p=10^{-6}$ Torr, there is no suggestion of a discontinuity at this point in the data. However, a slight positive curvature in these "isosteres" is indicated in Fig. 8. The worst case discrepancy from the lines presented is for $p=3.6\times10^{-6}$ Torr, for which both B and T_0^{-1} correspond to a somewhat higher pressure. In this n is wrong by $\Delta n=0.01$ ($\Delta m=0.005$) but generally $\Delta n\lesssim0.006$ or $\Delta m\lesssim0.003$. Systematic differences in p or T conditions between runs could account for this error Δm being somewhat higher than the 0.1–0.2 % measurement error on the diffraction patterns.

The data of Fig. 6 indicate an IA-IR transition at $m=1.5\pm0.5$ % corresponding to a coverage $n=0.97\pm0.01$. This is added to Fig. 8 as a dashed line. The angle of misorientation increases with decreasing density reaching $\simeq0.4°$ for the lowest density $n\simeq0.90$ studied. Recent single crystal x-ray work[23] indicated that the IA-IR transition occurred at about $m=1.9\pm0.3$ %, so we are almost certainly seeing the same transition, even though their pressures are not known.

The commensurate phase is clear on Fig. 8 as a thin region of the phase diagram, broadening as the pressure is reduced, and appearing to terminate as the $n=1.00$ line meets the bilayer line is a tricritical point in the region of $T=62.5\pm1$ K, $p=2.0\pm0.5\times10^{-6}$ Torr. In this same region there is a suggestion of a small excursion in the bilayer line as judged by the highest temperature points which have the characteristic bilayer misfit of 2.2 ± 0.1 % at the various pressures. It seems significant that previous LEED studies of Suzanne, Coulomb, and Bienfait[7] also observed a similar excursion in the same pressure region. This is shown dotted in Fig. 8.

A quantitative comparison of our results with the x-ray data is hampered by the fact that the two sets of experiments followed very different paths in the phase diagram. The x-ray experiments were carried out at a nominally constant coverage, or filling factor f, where $f=1$ corresponds to filling a C-phase monolayer; in general the pressure was not measured. In our case p and T are known but the coverage is obtained from Eq. (7), which assumes no vacancies or second-layer atoms. Thus $n=f$ only under those conditions, and we cannot continue our "isosteres" into the bilayer region. However, allowing for these differences, some comparison can still be made. Based on x-ray diffraction profiles obtained from Xe adsorbed on oriented powder graphite, Hong, Birgeneau, and Sutton[22] claimed that Xe never goes commensurate. Instead they interpreted their results in terms of an incommensurate-striped domain structure transition. This was inconsistent with previous THEED results and the causes of disagreements were discussed by Faisal *et al.*[12]

In a more recent publication, Hong *et al.*[23] used single-crystal graphite samples to study the adsorption of Xe at four different coverages, $f=0.90$, 0.96, 1.02, and 1.16. For the three highest coverages, which are relatively close to the monolayer-bilayer transition, they saw the commensurate phase at suitably low temperatures, thus confirming the previous THEED work.[10,11] However, there are still several points of apparent disagreement with the new THEED data, and with the phase diagram as drawn in Fig. 8. For example, at $f=1.16$ they reported that Xe undergoes three successive transitions as the temperature is lowered: a first-order aligned-rotated transition at ~117 K, then a continuous rotated-aligned transition at ~80 K, and finally a first-order I-C transition at 73 K. Assuming that these transitions are all at pressures close to the monolayer-bilayer line, the first two transitions are at pressures higher than those in Fig. 8. We have not examined these regions, although the present apparatus will allow us to do so in future. However, the third transition, marked H on Fig. 8, seems to sit somewhat uneasily on the same phase diagram as our data.

Any discrepancy between their results and ours concerns a very narrow region of the $(\log_{10}p-T^{-1})$ phase diagram at pressures very close to the bilayer line on Fig. 8. At $f=1.16$, the x-ray misfit data show that an I-C transition occurs at $T=73$ K with a jump in misfit from a value of $\sim1.2\%$ to zero. Our data indicate that above $T=62.5\pm1$ K, Xe is always observed to be incommensurate at the monolayer-bilayer transition while below this temperature the misfit goes to zero in continuous manner, as discussed in Sec. III B.

To reconcile these two observations it would be necessary that the C phase extends from 62.5–73 K at pressures very close to the bilayer line, but spanning a finite range of coverage. We clearly cannot rule this out from our data of Fig. 4. All that we can say is that we have never had the exact T and p conditions to observe the C phase in this region, and that the extrapolation of the higher T monolayer misfit data does not lead one to suspect such a phase. From the density of data points in Fig. 4, we think that any such phase must exist only ≤0.5 K from the bilayer line; assuming it does exist, it would have to be first-order transition, in contrast to the findings at lower pressures.

The differences in power laws quoted by the x-ray workers is due to the difference in paths through the phase diagram. Hong *et al.*[23] argue for $\beta=0.33$; but this is for the nominally constant coverage experiment (along, or close to, the bilayer line presumably) above point H on Fig. 8. Our data of Fig. 4 clearly show $\beta=0.80\pm0.03$ for nine experiments *at constant pressure.* There is no obvious reason why these two power laws should be the same, since the paths are very different. Detailed theories are needed to explain these values of β.

We feel sure that the power law deduced from the x-ray experiment[23] is bound up with the monolayer-bilayer transition is some way, as described above. At low temperatures where there are no vacancies or second layer atoms,[49,50] a truly constant coverage experiment would show no variation of the lattice parameter at all, as required by Eq. (7). However, their method of assuring constant coverage by using a large "ballast" of oriented powder graphite must have difficulties during a first-order event such as the monolayer-bilayer transition.

The coverage on the single crystal is mediated by the vapor pressure above the powder. Since by definition the pressure is constant in a first-order transition, it follows that this pressure can produce any coverage $1 \leq f \leq 2$; the coverage so produced will also be susceptible to (very small) differences in properties (e.g., steps, capilliary condensation) between the two samples, and to kinetic effects.

The comparison with results for krypton needs to be done carefully. A power law of the form of Eq. (2) is well established for the (negative) misfit observed in the monolayer region with $\beta = 0.32 \pm 0.02$.[40] It is reasonable to compare models of the *I-C* transition for Kr and Xe, since the main difference is in the sign of the misfit; in this sense our value of $\beta = 0.80 \pm 0.03$ is the xenon value to use, *not* the value quoted by the x-ray workers, because of the different position in the phase diagram. We argue elsewhere[48,51] that the prime driving force for the *I-C* transition is thermal expansion and that the anharmonicity involved does produce different values of the "exponent" in the sense observed.

The observation of diffraction spot broadening as the C phase is approached may have a bearing on theoretical studies of the domain-wall structures. If the broadening is thermodynamic in origin, the effect is possibly due to a distribution of domain sizes as described by the Villain picture of breathing modes.[52] If, instead, it is kinetic, the effect may be the result of a finite response (or relaxation) time of the monolayer. Recent theoretical models have shown that the domain wall spectrum has a gap, and consequently a finite relaxation time.[51,53] This would manifest itself ultimately in a finite response time of the 2D adlayer to changes in p and T. Further experimental work is in progress to determine if any time dependence of the broadening can be observed.

Nonetheless, it does seem that the phase diagram as presented in Fig. 8 is not the full story, and needs to be complemented by information as a function of the "third dimension," i.e., the coverage f which we do not measure directly in our experiments. At finite temperatures we can envisage the commensurate monolayer existing from $f = 1$ up to a given f_c between 1 and 2, with second layer atoms in the form of a dense fluid; above f_c there would be a first-order transition to the incommensurate bilayer. The recent x-ray work[23] suggests that this (commensurate monolayer plus fluid) exists up to temperatures considerably beyond our 62.5 K; the transition point we observe would then correspond to the temperature and pressure at which the *I-C* transition, which is second order at low pressures as shown here, becomes first order. The upward curvature in our isosteres would also be less marked if there is a substantial density (few percent of a monolayer) of second layer atoms at higher pressures. More detailed work is needed, however, to confirm these points and to elucidate the full extent of kinetic effects.

ACKNOWLEDGMENTS

We thank the Science and Engineering Research Council of the U.K. for supporting this work. Financial support for A.D.Q.F. from the University of Salah Aldeen (Iraq) and for M.H. from the Algerian Ministry of Higher Education is acknowledged. We are grateful to M. Hardiman, A. E. Curzon, and P. M. Horn for useful discussions and suggestions. The use of the PDS-Densitometer and Starlink systems at Herstmonceux is appreciated.

---

*Also at: Department of Physics, Arizona State University, Tempe, AZ 85287.

†Also at: Materials Science Center, University of Wisconsin, Madison, WI 53706.

[1]A. Thomy and X. Duval, J. Chim. Phys. **66**, 1966 (1969); **67**, 1101 (1970).

[2]J. Regnier, A. Thomy, and X. Duval, J. Chim. Phys. **74**, 926 (1977).

[3]Y. Lahrer and B. Gilquin, Phys. Rev. A **20**, 1599 (1979).

[4]N. J. Colella and R. M. Suter, Phys. Rev. B **34**, 2052 (1986).

[5]J. J. Lander and J. Morrison, Surf. Sci. **6**, 1 (1967).

[6]J. Suzanne, J. P. Coulomb, and M. Bienfait, Surf. Sci. **40**, 414 (1973); **44**, 141 (1974).

[7]J. Suzanne, J. P. Coulomb, and M. Bienfait, J. Cryst. Growth **31**, 87 (1975).

[8]J. L. Seguin, J. Suzanne, M. Bienfait, J. G. Dash, and J. A. Venables, Phys. Rev. Lett. **51**, 122 (1983); J. A. Venables, J. L. Seguin, J. Suzanne, and M. Beinfait, Surf. Sci. **145**, 345 (1984); M. Bienfait, J. L. Seguin, E. Lerner, J. Krim, and J. G. Dash, Phys. Rev. B **29**, 983 (1984).

[9]J. A. Venables, H. M. Kramer, and G. L. Price, Surf. Sci. **55**, 373 (1976); **57**, 782 (1976).

[10]J. A. Venables and P. S. Schabes-Retchkiman, J. Phys. **38**, C4-105 (1977); Surf. Sci. **71**, 27 (1978).

[11]P. S. Schabes-Retchkiman and J. A. Venables, Surf. Sci. **105**, 536 (1981); Inst. Phys. Conf. Ser. **41**, 329 (1978).

[12]A. Q. D. Faisal, M. Hamichi, G. Raynerd, and J. A. Venables, Phys. Rev. B **34**, 7440 (1986).

[13]E. M. Hammonds, P. Heiney, P. W. Stephens, R. J. Birgeneau, and P. M. Horn, J. Phys. C **13**, L301 (1980).

[14]P. A. Heiney, R. J. Birgeneau, G. S. Brown, P. M. Horn, D. E. Moncton, and P. W. Stephens, Phys. Rev. Lett. **48**, 104 (1982).

[15]P. A. Heiney, P. W. Stephens, R. J. Birgeneau, P. M. Horn, and D. E. Moncton, Phys. Rev. B **28**, 6416 (1983).

[16]T. F. Rosenbaum, S. E. Nagler, P. M. Horn, and R. Clarke, Phys. Rev. Lett. **50**, 1791 (1983).

[17]E. D. Specht, R. J. Birgeneau, K. L. D'Amico, D. E. Moncton, S. E. Nagler, and P. M. Horn, J. Phys. Lett. **46**, L561 (1985).

[18]P. Dimon, P. M. Horn, M. Sutton, R. J. Birgeneau, and D. E. Moncton, Phys. Rev. B **31**, 437 (1985).

[19]S. E. Nagler, P. M. Horn, T. F. Rosenbaum, R. J. Birgeneau, M. Sutton, S. G. J. Mochrie, D. E. Moncton, and R. Clarke, Phys. Rev. B **32**, 7373 (1985).

[20]K. L. D'Amico and D. E. Moncton, J. Vac. Sci. Technol. **A4**, 1455 (1986).

[21]K. L. D'Amico, J. Bohr, D. E. Moncton, and D. Gibbs, Bull. Am. Inst. Phys. **31**, 376 (1986).

[22]Hawoong Hong, R. J. Birgeneau, and M. Sutton, Phys. Rev. B

33, 3344 (1986).
[23]Hawoong Hong, C. J. Peters, A. Mak, R. J. Birgeneau, P. M. Horn, and H. Suematsu, Phys. Rev. B **36**, 7311 (1987).
[24]T. H. Ellis, S. Iannota, G. Scoles, and U. Valbusa, Phys. Rev. B **24**, 2307 (1981).
[25]T. H. Ellis, G. Scoles, and U. Valbusa, Surf. Sci. **118**, L251 (1982).
[26]G. Bracco, P. Cantini, A. Glachant, and R. Tatarek, Surf. Sci. **125**, L81 (1983).
[27]T. H. Ellis, G. Scoles, and Valbusa, Chem. Phys. Lett. **94**, 247 (1983).
[28]H. Jonsson, J. H. Weare, T. H. Ellis, G. Scoles, and U. Valbusa, Phys. Rev. B **30**, 4203 (1984).
[29]G. Bracco, P. Cantini, E. Cavanna, K. Tatarek, and A. Glachant, Surf. Sci. **136**, 169 (1984).
[30]T. H. Ellis, G. Scoles, U. Valbusa, H. Jonsson, and J. H. Weare, Surf. Sci. **155**, 499 (1985).
[31]For phonon studies of Xe/Ag(111) see K. D. Gibson and S. J. Sibener, Phys. Rev. Lett. **55**, 1514 (1985); for Xe/Pt(111), K. Kern, R. David, R. L. Palmer, and G. Comsa, Surf. Sci. **175**, L669 (1986).
[32]H. Jonsson, J. H. Weare, T. H. Ellis, and G. Scoles, Surf. Sci. **180**, 353 (1987).
[33]M. Bienfait, Surf. Sci. **89**, 13 (1979); in *Current Topics in Materials Science,* edited by E. Kaldis (North-Holland, Amsterdam, 1980), Vol. 4, p. 361.
[34]O. E. Vilches, Annu. Rev. Phys. Chem. **31**, 463 (1980).
[35]A. Thomy, X. Duval, and J. Regnier, Surf. Sci. Rep. **1**, 1 (1981).
[36]S. C. Fain, Jr., in *Chemistry and Physics of Solids Surfaces IV,* Vol. 20 of *Series in Chemical Physics* (Springer-Verlag, Berlin, 1982), p. 203; S. C. Fain, Jr., M. F. Toney, and R. D. Diehl, *5th International Conference on Solid Surfaces, Madrid, 1983* (Asociacion Española del Vacio y sus Aplicaciones, Madrid, 1983), p. 129.
[37]L. W. Bruch, Surf. Sci. **125**, 194 (1983).
[38]R. J. Birgeneau and P. M. Horn, Science **232**, 329 (1986).
[39]C. G. Shaw, S. C. Fain, Jr., and M. D. Chinn, Phys. Rev. Lett. **41**, 855 (1978).
[40]S. C. Fain, Jr., M. D. Chinn, and R. D. Diehl, Phys. Rev. B **21**, 4170 (1980).
[41]S. Calisti and J. Suzanne, Surf. Sci. **105**, 255 (1981); S. Calisti, J. Suzanne, and J. A. Venables, *ibid.* **115**, 455 (1982).
[42]L. L. Levenson, Comptes Rend. (Paris) **B265**, 1217 (1967).
[43]J. A. Venables, A. Q. D. Faisal, M. Hamichi, M. Hardiman, R. Kariotis, and G. Raynerd, Ultramicroscopy **26**, 169 (1988). published).
[44]J. E. Bartmess and R. M. Georgiacodis, Vacuum **33**, 149 (1983).
[45]In Ref. 12 we referred to this point as a triple point. However, it is more correctly referred to as a tricritical point, where a line of second-order transitions runs into a first-order transition line [see, e.g., I. D. Lawrie and S. Sarbach, in *Phase Transitions and Critical Phenomena,* edited by C. Domb and J. L. Lebowitz (Academic, New York, 1983), Vol. 9, p. 2].
[46]A. D. Novaco and J. P. McTague, Phys. Rev. Lett. **38**, 1286 (1977).
[47]H. Shiba, J. Phys. Soc. Jpn. **46**, 1852 (1979); **48**, 211 (1980).
[48]R. Kariotis, J. A. Venables, M. Hamichi, and A. Q. D. Faisal, J. Phys. C **19**, 5717 (1987).
[49]G. L. Price and J. A. Venables, Surf. Sci. **59**, 509 (1976).
[50]B. Mutaftschiev, Surf. Sci. **61**, 93 (1976).
[51]R. Kariotis, J. A. Venables, and J. J. Prentis, J. Phys. C **21**, 3031 (1988).
[52]J. Villain, in *Ordering in Strongly Fluctuating Condensed Matter Systems,* edited by T. Riste (Plenum, New York, 1980), p. 221.
[53]F. Marchesoni and C. R. Willis, Phys. Rev. A **36**, 4559 (1987).